SAND2013-0426C

LNG SHIP INSULATION EXPERIMENTS USING LARGE LNG POOL FIRE BOUNDARY CONDITIONS

Thomas Blanchat, Charles Morrow, and Michael Hightower

Sandia National Laboratories[1]

Keywords: LNG, pool fire, carrier, insulation

Introduction

The increasing demand for natural gas is expected to increase the number and frequency of Liquefied Natural Gas (LNG) tanker imports and exports at ports across the U.S. Because of the increasing number of shipments and facility siting applications, concerns about the potential for an accidental spill or release of LNG have increased. In addition, since the incidents surrounding September 11, 2001, concerns have increased over the impact that accidents and other events on hazardous or flammable cargoes, such as those carried by LNG ships could have on public safety and property. The risks and hazards from an LNG spill will vary depending on the size of the spill, environmental conditions, and the site at which the spill occurs. Risks could include injuries or fatalities to people, property damage to both the LNG ship and equipment and onshore property, and economic impacts due to long-term interruptions in the LNG supply or closure of a harbor. With the growing use of LNG to meet increasing natural gas demands, damage or disruption from a spill at LNG terminals or harbor facilities could curtail LNG deliveries and impact natural gas supplies. Therefore, methods to ensure the safety, security, and reliability of current or future LNG terminals and LNG shipments are important from both public safety and property perspectives, as well as from a national and regional energy reliability standpoint.

As LNG imports started to increase in the U.S. in the early 2000's, a number of hazard studies were conducted that resulted in widely varying consequence and hazard estimates resulting in broad public concern over the adequacy of hazard and consequence analysis techniques. Subsequent Sandia analysis [Hightower et al. 2004] highlighted some primary knowledge gaps that were limiting the fidelity of site-specific risk assessments due primarily to the lack of large-scale LNG spill, fire, and damage data. Experimental studies used to justify hazard analyses were 10 to 100 times smaller in scale than potential incidents. The limiting factor in conducting the needed larger-scale experiments was that they were thought to be cost prohibitive.

While much progress has been made in LNG threat, consequence and vulnerability assessment; for example, a general approach to risk evaluation has been developed and used for a basis in site-specific risk assessments [Hightower et al. 2004]; there are still knowledge gaps for very large scale LNG pool fires [Luketa et al. 2008] that limit the fidelity of site-specific risk assessments and remain a focal point of concern. These knowledge gaps result in the need to make assumptions in hazard analysis that may or may not be warranted and could lead to over predicting or underestimating hazards and impacts to the public, property, the economy, or energy reliability.

To address these concerns, the United States Congress funded the US Department of Energy (DOE) in 2008 to conduct a series of laboratory and large-scale LNG pool fire experiments at Sandia National Laboratories (SNL or Sandia) in Albuquerque, New Mexico. The focus of the LNG pool fire testing efforts were to improve the understanding of the physics and hazards of large LNG spills and fires by conducting laboratory experiments and fire tests of LNG spills, on water, producing pools of up to 100 m in diameter. These tests were expected to better represent the fire behavior of spills postulated from current and future LNG carriers.

Due to its unique chemistry, methane fires behave differently compared to other hydrocarbon fuel fires, but are expected to follow the trend of heavy hydrocarbon fuel fires, where the surface emissive power (SEP) of a pool fire increases to reach a maximum value then decreases to reach a limiting value with increasing diameter. For LNG, the limiting SEP value is unknown and verifying the actual values required the improved laboratory and large-scale experiments funded by the US Congress. These large scale spreading LNG pool fire experimental datasets, combined with small-scale gas-burner experiments, support pool fire model

[1] Sandia National Laboratories is a multi-program laboratory managed and operated by Sandia Corporation, a wholly owned subsidiary of Lockheed Martin Corporation, for the U.S. Department of Energy's National Nuclear Security Administration under Contract DE-AC04-94AL85000.

development and validation for extrapolation to a scale of an potential LNG spill of 200-400 m or larger in diameter [Luketa 2011].

Objectives of the Paper

Concern over the vulnerability of Liquefied Natural Gas (LNG) carriers entering US ports has increased in recent years. Several studies have weighed in on the potential consequences resulting from large accidental or intentionally caused spills. One specific concern was that LNG cargo tank insulation could be susceptible to high-temperature thermal degradation in the event of a large-scale LNG fire. This could result in cascading damage of other cargo tanks not originally damaged during an initial accident or intentional event, with the concern that this cascading damage could cause much larger spills and increase hazards to the public and property. To address this concern, part of the US Congress funding was directed by DOE for Sandia to conduct a series of tests on the thermal degradation during large fires of representative insulation systems installed on LNG carriers.

This paper will briefly describe the goals, methods, and results of the two LNG pool fire tests that provided fire boundary conditions for the carrier insulation tests. This paper will also summarize the test methodology, data, and results of four experiments that tested insulation systems for both Moss and Membrane LNG carriers at for large LNG pool fire conditions. Finally, this paper will summarize analyses that were performed to determine the impacts from fires for both membrane and Moss cargo tanks, such as relief valve sizing, vessel pressure containment capability and other thermal issues.

Large-scale LNG Pool Fire Experiments

A key technical element in establishing hazard distances from fires is establishing the surface emissive power (SEP) of the fire. One of the deficiencies of historical data is due to the small scale of the fires (10 to 100 times smaller) relative to possible spill diameters, particularly when the SEP is a strong function of fire diameter. The principal reason for the small fire diameters was cost. Cost estimates to build a facility to conduct large-scale LNG pool fire tests were prohibitive. This forced Sandia to assess ways to develop a safe, low-fabrication-cost experimental setup. The selected solution necessitated significant operational safety considerations including unprecedented cooperation between numerous Sandia organizations, the DOE Sandia Site Office, and Kirtland AFB agencies (including flight-operations and emergency fire-response). By focusing on the experimental objectives, and using experience in conducting large-scale experiments, the team came up with a-simple, low-cost experimental approach that enabled testing at an appropriate scale. The experimental design concept (Figure 1) included: 1) using the soil excavated from the creation of a shallow 120-m diameter pond to create a deep, 310,000 US gallon reservoir to hold the LNG while filling, 2) insulating and covering the reservoir to minimize vaporization losses, 3) using industry standard prefabricated reinforced concrete pipes to transport the LNG from the base of the reservoir to the center of the pool, and 4) using a simple, liftable plug to allow gravity and the reservoir geometry to control the flow rate.

Figure 1. The Large Scale LNG Pool Fire Experimental Site

This approach enabled high LNG flow rates onto water representative of potentially large spills, while minimizing the need for cryogenic rated high-flow rate pumps and hardware. This approach required significant environment, safety, and health analysis to provide confidence that the design and operations would be safe. Safety issues examined included reservoir integrity, thermal (cryogenic to fire fluxes) impacts, asphyxiation, explosion, drowning, and aviation operations (helicopter and airport traffic) issues. Advanced transient, three-dimensional transport simulations were used to estimate both the thermal performance of the reservoir and components, the transport of gaseous boil-off during the cool-down process, and in the design

of the diffuser in the middle of the pool needed to translate the linear momentum of the LNG in the discharge pipes into a radially spreading pool.

The large-scale LNG spill tests were performed with liquid methane (>99.5%) as a surrogate for Liquid Natural Gas (LNG) to minimize the potential for explosive rapid phase transitions (RPTs) and to reduce uncertainty in the analysis of the test data and better support future model development and validation. Previous historic experiments performed with typical LNG have shown that the methane burns off first, and therefore there is no impact on fire results..

Two experiments were completed obtaining fires from LNG spills with spreading pool diameters of approximately 21 m and 83 m. Extensive sets of fire data were collected for each test. Numerous cameras, spectroscopic diagnostics, and heat flux sensors were used to obtain heat flux data from the resulting fires. The spreading pool fire area was photographed with the aid of gyroscopically stabilized cameras deployed in U.S. Air Force helicopters. While three tests were proposed and attempted (to achieve spreading pool diameters at ~35 m, 70 m, and 100 m), it is believed that the data collected from the two successfully completed tests is sufficient to allow spill and fire model development and validation for use in estimating hazards and consequences for LNG pool fires on water with diameters of 200-400 m.

The data collected showed some unique and unexpected results, specifically that the fire diameter was not the same as the spreading pool diameter as had been assumed by all analyses to date. Previous studies with stagnant pools in pans had resulted in fires the same size as the pool. However, in all such studies, the pans have edges that can result in flame stabilization that would not be available on the open water. The data collected further showed that in both very light and significant cross-winds the flame will stabilize on objects projecting out of the fire, suggesting that the ship itself will act as a flame anchor.

In LNG Test 1, 58.0 m^3 (~15,340 gal) were discharged in ~510 s through a 15-inch discharge pipe. The flow rate initially was about 0.061 m^3/s (970 gpm) and increased throughout the test, reaching 0.123 m^3/s (1960 gpm) at the end of the test. During the steady-state fire interval of 390-510 s, the average flow rate from the reservoir was 0.121 m^3/s (1921 gpm), yielding an average mass discharge rate of 50.8 kg/s from the reservoir. The liquid mass flow rate from the diffuser was slightly less at 49.4 kg/s due to 2-phase flow and the generation of methane vapor. The steady-state pool area yielded an equivalent circular diameter of 20.7 m. At steady-state, the average regression rate of the burning pool was 0.147 kg/m^2s.

In LNG Test 1, the average wind speed was 4.8 m/s from a direction of 331 degrees, tilting the flame plume to the South. The average length was ~70 m (as compared to an average height of ~34 m). The average tilt angle was ~50°, yielding an L/D ratio of ~3.4. Narrow view (spot) radiometers corrected for transmission losses measured a spot-average steady-state surface emissive power (SEP) of 238 kW/m^2. A flame-average SEP was determined by correlating view factor information from video analysis with the wide-angle radiometer data, yielding an average overall SEP of 277±60 (2σ) kW/m^2.

In LNG Test 2, about 198.5 m^3 (52,500 gallons) were discharged in ~144 s through the three discharge pipes. The average flow rate during the fully open period (130 s to 220 s) was 1.91 ± 0.84 m^3/s (30300 ± 13350 gpm), yielding a mass discharge rate of ~802 kg/s. The spreading LNG pool area continuously increased during the discharge interval, achieving an equivalent circular diameter of ~83 m at the end of the spill. Since the reservoir emptied prior to the pool achieving a constant area, a burn rate could not be calculated.

The test had unexpected results in that the fire did not attach to the leading edge (upwind and both sides) of the spill, hence the effective fire diameter was smaller than the spreading LNG pool diameter. The average flame width at 15 m above the pool was ~56 m and the average flame height was ~146 m during the steady-state interval from 250-300 s. This yields an H/D ratio of ~1.7 and an H/W ratio of ~2.6. The average wind speed was 1.6 m/s from a direction of 324 degrees. There was very little flame tilt; however, the wind did appear to drag the plume toward the south.

Narrow view (spot) radiometers on the North and South data collection spokes yielded spot-average steady-state surface emissive power (SEP) of 316 kW/m^2 and 239 kW/m^2, respectively. The SEP on the South spoke is believed to be low due to the presence of smoke from grass fires partially obstructing the view of the instruments. The overall flame average SEP was 286±20 (2σ) kW/m^2.

Thermal radiation spectra as a function of height and time were acquired using a scanning mid-infrared (1.3-4.8μm) spectrometer. For LNG Test 2, data reduction efforts were concentrated on spectra acquired within the quasi-steady burning period (250-300 sec). The spectra from heights at approximately ground level to ~100 m yielded thermal radiation intensities lowest for elevations closest to the ground and then increased

steadily to a maximum where they remained until the maximum scan height was achieved. There was no indication of declining intensities at the maximum scan height (103 m).

Analyzed spectra determined that the dominant contributor to the thermal radiation was from broadband soot emission. The overall thermal radiation reaching the spectrometer was attenuated by atmospheric water and CO_2 which resulted in a decrease in intensity at different wavelength bands. In LNG Test 2, at heights above ground from ~40 m to 103 m (the top of the measurement region above the pool), the data was fairly consistent, with spectra-derived flame temperatures between 1300-1600°C and emissivity between ~0.3-0.4.

The agreement in the surface emissive power derived from the radiometer data and the spectrometer data was found to be acceptable and within the experimental variability. Surface emissive power (from spectrometer data) was a minimum near the ground level, with approximate values of 100 kW/m^2. The SEP then increased steadily from 0 to 40 m and reach peak values approaching 275 kW/m^2.

Additional spectrometer data was collected with an FTIR spectrometer, a high-speed visible camera, and a thermal imager. A two-temperature spectra fire model correlated extremely well to the measured spectra. It is postulated that the two temperature states more accurately depict the true nature of the fire by characterizing both the efficient combustion regions and those dominated by slow burning, absorbing soot.

Figure 2 plots SEP vs. LNG pool diameter for a variety of hydrocarbon fuels [Vela 2009, except for current data], including the three SNL LNG pool spread tests on water (including an earlier SNL 2005 10 m test). SEP for hydrocarbon fuels all have similar behaviors in that the SEP starts low (due to burning in a laminar regime), increases as the burning transitions into a fully-turbulent regime), and then tails off due to smoke shielding as soot is quenched at the flame surface. Soot quenching starts at the flame mantle, and as the fire size increases, the smoke shield progressively moves down towards the base of the burning pool. LNG is expected to follow similar trends; however, due to its unique molecular bond structure, the shape of the curve is shifted toward the right as indicated by the test data.

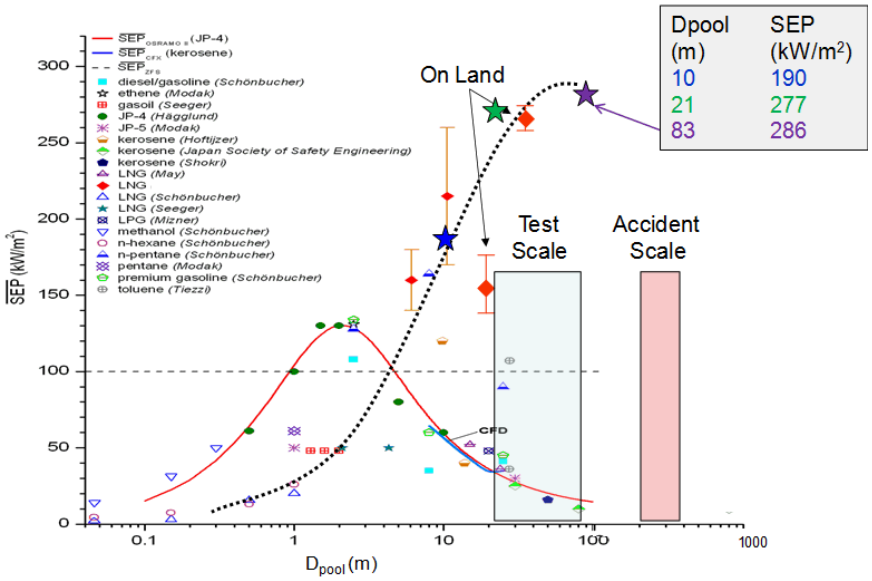

Figure 2. SEP vs. pool diameter for various hydrocarbon fuels.

Figure 3 shows three LNG tests performed at SNL on water, captions indicate the effective diameter of the LNG spreading pool (all tests were performed with high-purity methane). Even though very little smoke shielding occurred in any of the tests, the trend in the data (Figure 2) does indicate that the SEP is leveling off, indicating that a SEP of ~286 kW/m^2 can be expected for spreading pools with diameters in the range of 100 m, and would be a reasonable value for use in hazard calculations for structures adjacent to or near the fire. Larger LNG fires are expected to have smoke shielding effects in the upper portions of the flame plume that will lower the SEP. This would impact hazard calculations for far-field objects but not for near-field objects relatively close to the base of the fire.

Smoke mantles were not evident in either test. There were a few instances when small amounts of smoke were seen in LNG Test 2 during the production of large scale vortices that “rolled up” from the base of the flame when the fire exhibited a puffing behavior, as can be seen in Figure 3.

The results from LNG Test 2 identified a number of pool fire dynamics that should be considered when modeling flame spread on the LNG pool surface, flame geometry, and smoke production for use in hazard predictions. They include 1) water entrainment and condensation in the cold region above the pool acting as a suppressant, 2) entrapment of methane in hydrates (forming with water in the pool) that limit the fuel supply rate, 3) air in-flow velocity from both air entrainment created by the intense fire and ambient wind opposing flame spread, 4) de-coupled LNG pool spreading and fire spreading, and 5) lack of flame anchoring over the water pool.

The LNG pool fire size, soot production, and SEP could vary depending on the size of a harbor and the relative congestion. Flame anchoring could change fire dynamics, behavior, and hazards. The de-coupling of the flame spread with the pool spread, i.e., lack of flame anchoring to the leading upwind edge of the spreading LNG pool over the water pool, was evident in all three spreading LNG pool fire tests performed at Sandia, shown in Figure 3. Fire models that capture the above dynamics will be needed to better understand LNG fire physics and behavior over water.

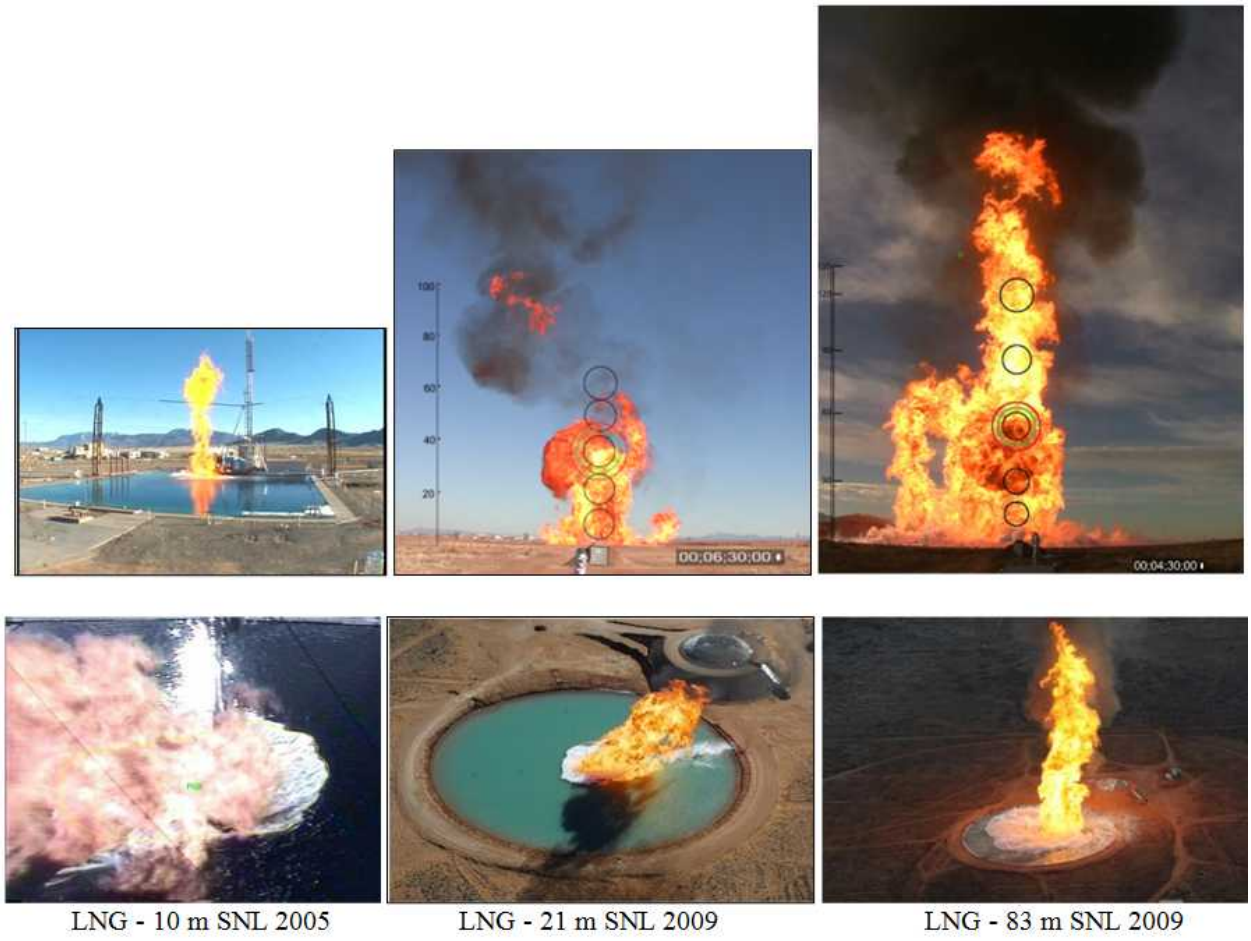

Figure 3. LNG fire dynamics at large scale.

Large-scale LNG Carrier Insulation Experiments

Most risk assessments suggest that the breach of multiple LNG carrier tanks is unlikely, but there is concern that an engulfing LNG pool fire resulting from the breach of one tank could lead to damage of neighboring tanks (i.e., cascading damage). The primary purpose of the insulation is to control boil off of LNG during normal operations. This insulation, while not installed for fire protection, does have an effect on design considerations related to fire, specifically related to the sizing of pressure relief valves on cargo tanks. The primary goals of the experimental study were to:

1. Determine the rate of decomposition of LNG tank cryogenic insulation systems and determine whether further investigation into potential consequences is warranted.
2. Improve the understanding of the consequences associated with the thermal damage and decomposition of cryogenic insulation.

3. Estimate the relationship between the applied heat flux associated with a fire and insulation decomposition rate. In a one-dimensional (1D) heat transfer analysis the insulation decomposition rate can be expressed as a thermal front velocity. Obtaining empirical data on the rate of decomposition of representative insulation systems as a function of heat fluxes allowed for comparison of different systems and supports estimating the time required for insulation systems to decompose in fire scenarios.
4. Assess insulation degradation impacts on cargo tank pressures and damage.

There has been a view that the LNG cargo tank insulation could rapidly decompose during a large-scale LNG pool fire. Some models, based on transient analysis and theoretical approximations, supported these conclusions. Other models showed opposite results. Experimental studies on actual LNG carrier insulations were needed to improve damage modeling results which could vary based on the insulation system, the type of carrier, the type of insulation, and the location on the cargo tank.

Several LNG carrier and cargo tank designs exist and are in operation today, and each has several available insulation systems, some of which are no longer in production. Priority was given to testing representative insulation systems of greatest interest to the DOE and the USCG. It must be noted that LNG ship cryogenic insulation systems are not designed to resist high temperatures, especially those resulting from a large LNG breach, spill and fire. The purpose of the insulation materials is to preserve the cold condition of the cryogenic LNG cargo. The representative insulation materials tested complied with all relevant industry codes and regulations. The materials are classified as fire retardant or self-extinguishing according to recognized standards.

Most of the Moss ships have 5083 aluminum tanks. Sphere thickness varies from 30 mm to 65 mm, with the thinnest portions near the top of the tank. The cargo tank hold sits within the inner hull and has a steel weather cover under which the insulated cargo tank is located. The cargo tank hold is normally filled with dry air, but can be inerted in the event of a cargo leak into the space. This annular space width varies, having its greatest width, approximately 1.5 m, near the weather deck. Typical materials used in Moss LNG insulation systems include polystyrene, polyurethane and phenolic resin foams. These are considered combustible to slightly combustible and will burn when exposed to an open flame. These begin to decompose at temperatures around 550°K (277°C). Foams decompose very differently when exposed to the open atmosphere as opposed to being in an enclosed space with limited availability of oxygen. Therefore, close attention was paid in conducting these tests at expected operational conditions.

A common Moss insulation system consists of multiple layers of extruded or expanded polystyrene with an aluminum foil vapor barrier on the outside. Typically, glass fiber mesh cloth reinforcement is glued between layers in the insulation. Another insulation system used for Moss LNG carriers uses polyurethane foam (PUF) panels or polystyrene panels or a composite panel system fabricated from a layer of polyurethane foam (PUF), a steel wire net (mesh) crack arrestor, and a layer of phenolic resin foam (PRF) attached by aluminum studs to the cryogenic tank wall. All the insulation systems are designed to control the boil off rate, typically in the range of 0.10-0.15%/day. .

A membrane LNG cargo tank system is formed by installing thermal insulating material on the inner hull structure of the ship and covering it with a thin membrane secondary barrier, a further layer of insulation is then installed which is covered by the primary membrane (in contact with the LNG). The secondary membrane is required to be liquid tight for a period of 15 days in the event of a failure of the primary barrier. The load of the cargo liquid acts directly on inner hull (transferred through the insulation system). In the event of membrane leakage, two relief valves are normally installed on both the interbarrier space and insulation space. The double hull structure of a membrane LNG carrier continues above the deck level, completely surrounding the cargo tank. The inner hull steel thickness is ~14 mm thick and the outer hull steel thickness is ~23 mm thick, with a separation between the hulls of ~2 m.

The predominant membrane insulations are the GTT (GazTransport and Technigaz) Mark III and the GTT No96. The cargo tank and insulation for a GTT Mark III consists of two polyurethane foam panels separated by a composite secondary membrane. The primary membrane is ~1.2 mm thick stainless corrugated steel. The membrane is fitted and welded to stainless steel strips built into the insulation panels. The insulation system is comprised of three layers glued together: a secondary polyurethane foam panel reinforced with a fiberglass mat glued to a plywood board, a composite material layer that acts as secondary barrier, and the primary polyurethane foam layer reinforced with fiberglass mat attached to a plywood board. The insulation panels are glued to the inner hull of the carrier with mastic ropes that also function to support the insulation and the membranes. Additionally the mastic ropes compensate for any inner hull unevenness.

The cargo tank and insulation for a No96 system is based on two identical membranes made of Invar (both ~0.7 mm thick). Invar is a 36% nickel steel alloy with a very low shrinkage coefficient, about 10 times less

than that of steel. The insulating elements, both primary and secondary, are plywood boxes filled with perlite. Perlite is an insulation material based on expanded silica. The secondary boxes are bolted to the inner hull and are set against mastic ropes, which compensate for the lack of flatness of the inner hull and provide the necessary bearing surface. A sheet of craft paper rests between the resin and the inner hull to allow the boxes free movement for hull deflection.

Insulation System Experiment Design and Methodology

The large scale experiments were designed to determine the rate of insulation system decomposition for typical Moss and membrane LNG carrier cargo tank insulation systems. Attention was focused on testing insulation representative of locations above the waterline and at or above the deck level, where high heat fluxes and thinner walls (hulls or weather covers) occur.

Experiments were conducted at the Sandia's Thermal Test Complex (TTC) Radiant Heat Facility. The test facility uses banks of electrically-powered tungsten heat lamps capable of achieving temperatures of 2700 K. Lamps can be oriented in any direction. The facility can field up to 24 water-cooled aluminum flat panel lamp holders (1.17 m (46 inch) tall x 0.305 m (12 inch) wide), each holding 63 tungsten lamps (6 kW apiece), arranged in flat or curved arrays providing a total heated area of 8.6 m^2. The rated electrical power capacity of the facility is ~5.2 MW. The use of these heat lamps provides the ability to accurately control the heat flux in each experiment, providing very reproducible tests so that system performance can be easily compared among different insulation systems.

Typically, the lamps heat Inconel shrouds that then radiate to the test object. With temperatures limited to about 1300K to prevent damage to the Inconel shroud, heat fluxes in the range of 150 kW/m^2 are produced. To achieve higher heat fluxes, the system is operated in a "direct shine" mode, where the lamps radiate directly onto the test article. Figure 4 shows the 4-panel flat radiant heat array (bare lamp mode) used in the tests. Each panel was fully lamped, producing a radiative surface area of about 1.4 m^2 at a power capacity of 1.5 MW.

For each test, a representative insulation system or panel was inserted inside an insulated test enclosure. The test enclosure (also shown in Figure 4) was designed to produce an approximately 1D thermal response through the center of each insulation system (or test panel) when the lamp array is positioned close to the face of the enclosure. At the rear of the enclosure, each test panel was attached or butted against an aluminum tank filled with liquid nitrogen (LN_2), that acts as a LNG surrogate to produce a simulated cargo tank cryogenic boundary condition (-196°C vs. -160°C) for each insulation system. The test enclosure, which is essentially an insulated box, was designed to be reused, with relatively easy removal and replacement of each test panel. Nominal dimensions of the interior of the enclosure are 1 m wide and 1 m tall, with a depth (to provide a hold space representative for a Moss carrier or a void (ballast) space representative for a membrane carrier) dependent on the insulation system being tested. This testing approach provides the capability to test large, representative insulation systems.

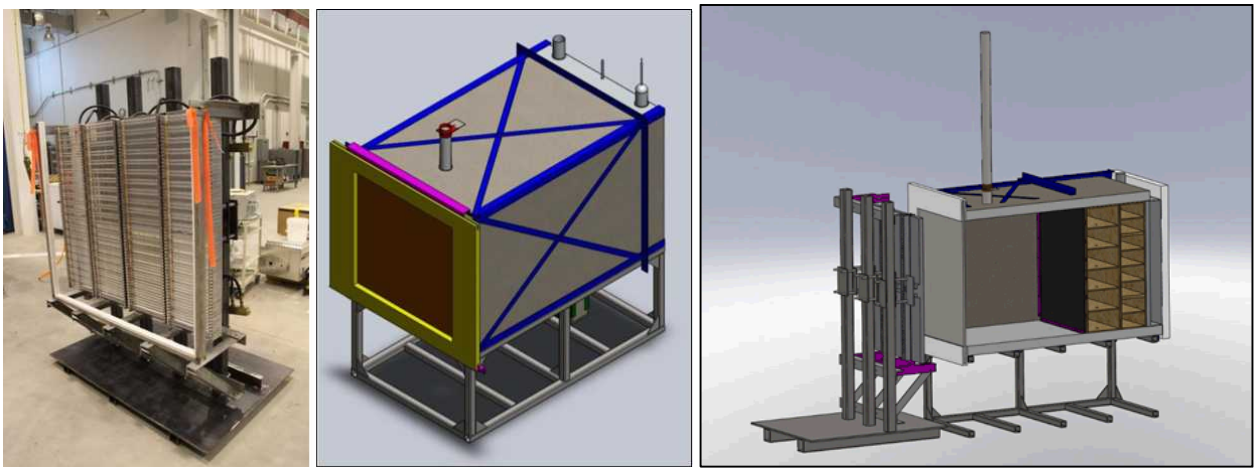

Figure 4. Insulation System Experiment Design.

The enclosure floor, walls, and ceiling were fabricated using 3 inch thick Pyrotherm I-series board, a low density hydrous calcium silicate board featuring exceptional strength and low thermal conductivity. Inorganic and incombustible, I-series boards contain no refractory ceramic fibers and can withstand temperatures up to 1093°C. The emissivity of the board is ~0.9.

The front of the enclosure supports a steel plate representing either a weather cover for the Moss LNG tanks or the outer hull of the membrane carrier. An insulation mask is fitted over the steel plate (providing a 1 m x 1 m heated area) to reduce heat to the enclosure steel frame. The emissivity of the oxidized steel plate is ~0.7.

In typical insulation systems, there is not enough air to support significant combustion. In fact, all of the systems have a small nitrogen bleed specifically used to sweep through and monitor for LNG leaks. As part of the pretest and cool down procedures, a nitrogen purge system removed the majority of the oxygen within the enclosure prior to testing. The nitrogen purge was continued both during the test and during the posttest cool down to ambient conditions. As many of these insulation materials produce combustion products as they decompose, a vent was placed at the top of the enclosure to prevent over pressurization.

As discussed, an aluminum tank filled with liquid nitrogen provides the cryogenic LNG cargo tank boundary condition. The tank was 1 m wide by 1 m tall by 102 mm deep. The thickness of the wall facing the test panel was 38 mm; all other walls were 6 mm thick. Two openings at the top were used for filling, venting to preclude over-pressurization, and access for a liquid level system.

Thermocouples were installed in each insulation system (divided into six to nine planes, with between six to thirteen thermocouples per plane) to measure the temperature distribution and determine the thermal front velocity. Thermocouples were also placed on the steel plates representing the weather cover and hull plates.

Thermocouples were also attached to the front face (adjacent to the insulation test panels) of the aluminum tank that contains the liquid nitrogen. The tank was milled with a 1.6 mm groove (for the TCs) to allow the insulation systems to lay flush with the tank surface. Additional thermocouples measured the test enclosure walls and air temperatures.

All thermocouples (TCs) were type-K, 1.6 mm diameter, mineral-insulated, metal (Inconel) – sheathed (MIMS). Thermocouple data was collected at a time interval of 1 Hz to allow for estimation of thermal front velocity. The overall uncertainty of the temperature measurements are assumed to be ±3ºC, which adds some conservatism to the ANSI standard uncertainty over the expected range of temperatures.

Heat flux to the weather cover or outer hull plate was measured with a radiometer (Medtherm model 64-30sb-18K/sw-1c-120, 120º view angle, 0-300 kW/m^2 range). The overall uncertainty of the radiometer flux measurements, based on manufacturer's calibration, is ±3%.

The distance from the lamps to the plate representing the weather cover or the outer hull is ~13.5 inches and the distance from the lamps to the face of the radiometer is ~6 inches. Due to the 120º view angle, the radiometer sees only the lamps (a circle of ~24 inches). The view factor of the heated plate to the lamp array is ~0.64; however, the effective view factor approaches a value of 1 due to the addition of the high emissivity insulation boards that enclose the heated region on the bottom and both sides.

Heat flux into the center front face of the aluminum cryogenic tank was measured by an RdF micro-foil heat flux sensor (RdF model 27036-1, nominal sensitivity 50.7 μV/kW/m^2, max flux 567 kW/m^2, 0.4 s time constant, temperature range -184°C to 149°C) with integral type-T thermocouple. The gauge was placed on the aluminum tank front face center and fixed with Kapton tape.

A liquid level system (Helium gas bubbler and dip-tube) measured the pressure head of the LN_2 in the tank, and was converted to a liquid level measurement to measure boil-off. The source gas was a 44 liter bottle of helium, coupled to a high precision regulator, a precision adjustable flow valve, and a flow meter; which the fed a bubbler exhausting at the bottom of the aluminum tank. Line pressure was measured using a 50 inch water column/differential pressure gauge (±1% full scale accuracy).

The TTC facility Process Equipment Control System (PECS) monitored and recorded the power (volts and amperes) supplied to the four lamp assemblies for each test. Three video cameras were used view outside of the test enclosure (top and two sides) during each test.

Insulation System Preparation for Testing

Four insulation system fire damage tests were conducted; the insulation system for each test is listed in Table 1. Either drawings and specifications for the panels and assembly were provided to Sandia or actual panels were provided by the insulation manufacturers for both the Moss and membrane insulation systems. Specifications and fine details are not provided here due to the proprietary nature of much of the information; however, some pictures are provided to allow understanding of the scale and magnitude of the effort.

Table 1 Insulations Systems Test Matrix

Test	Insulation System
1	Membrane – No96 perlite-filled plywood boxes
2	Membrane – MK III polyurethane foam panels
3	Moss – Polyurethane foam/ phenolic resin foam (PUF/PRF) composite panel
4	Moss – Extruded polystyrene (EPS) panel

NO96 Panel Procurement and Instrumentation

Drawing and specifications for the panel and assembly were provided to Sandia and Sandia obtained all materials. Glues and mastics were prototypic; the glue used for the bonding of the stainless steel sheet between the two wood boxes was a bi-component polyurethane-based adhesive and the epoxy mastic used to bond the secondary box to the inner hull was a bi-component resin and hardener system. Note that the bonding of the stainless steel sheet was typical of the test set up only, such bonding does not actually occur in the No96 system. Assembly of the boxes was in accordance with the ABS 2008 “Guidance Notes on Surveys during Construction of Membrane Tank LNG Carriers” and additional instructions from GTT.

The No96 configuration included a heated area of 1000 mm x 1000 mm (the steel outer hull plate, ~23 mm), a gap between outer hull and inner hull (~1065 mm), the steel inner hull plate (~14 mm) glued to the perlite-filled secondary plywood box (~0.3 m deep) set against resin beads, a stainless-steel membrane (~0.7 mm), the perlite-filled primary plywood box (~0.2 m deep), and the aluminum cryogenic tank (38 mm wall thickness) which was covered with polystyrene insulation on the back side (51 mm) to reduce boil-off.

Care was taken during the perlite fill to obtain prototypic size distribution and density (~50-65 kg/m^3) in the primary and secondary boxes. Figure 5 shows a few photographs taken during the assembly of the No96 test panel. They include the perlite fill, thermocouple layout and installation on the secondary box, gluing the thin steel membrane (representing the Invar membrane) between boxes, and final assembly of the insulation system.

Figure 5. No96 Insulation System Assembly.

GTT MK III Panel Procurement and Instrumentation

Drawings and specifications for the panel and assembly were provided to Sandia by GTT. Glues and mastics were prototypic. Assembly of the insulation system was in accordance with “Guidance Notes on Surveys during Construction of Membrane Tank LNG Carriers” and additional instructions from GTT. An insulation supplier for GTT fabricated and supplied the MK III material (RPUF bonded to Type A Plywood and also the HRT-2001 rigid secondary barrier (glass cloth embedded with a resin matrix molded to both sides of a thin aluminum foil)).

The GTT MK III configuration included a heated area of 1000 mm x 1000 mm (the steel outer hull plate, ~23 mm), a gap between outer hull and inner hull (~1319 mm), the steel inner hull plate (~14 mm), the three-layer insulation panel (the secondary insulation, an ~10 mm thick plywood board glued to ~200 mm thick polyurethane foam reinforced with fiberglass, panel is glued to the inner hull with mastic rope), the rigid primary insulation, an ~100 mm thick polyurethane foam reinforced with fiberglass glued to an ~10 mm thick

plywood board), the aluminum cryogenic tank (38 mm wall thickness), and the polystyrene insulation on aluminum tank back side (51 mm).

Final assembly of the MK III insulation system was performed in a similar manner as for the No96 system. The composite secondary insulation panel was glued to the inner hull plate. The same type of glue was used to bond plywood to foam and foam to the rigid composite secondary membrane. Specifications for pressing time, temperature, and pressure were provided by GTT.

Small diameter holes (~5 mm) were drilled into the foam to depths appropriate for the location of thermocouples; a fixture guided the drill bit and provided accuracy of ±2 mm at the maximum depth of 500 mm. Depending on the location, one, two, or three thermocouples were insert to the correct depth and glued in place. Figure 6 shows a few of No96 panel insulation system assembly photographs. They include the thermocouple layout and installation on the primary foam/wood panel, gluing the thin composite secondary membrane between foam panels, gluing the primary and secondary panels including the final press and cure, and laying the mastic resin in preparation to attachment of the inner hull steel plate.

Figure 6. MK III Insulation System Assembly.

Moss Polyurethane Foam/Phenolic Resin Foam Composite Insulation Panel Procurement and Instrumentation

Procurement of the phenolic resin/polyurethane composite insulation panel was facilitated by Moss Maritime AS. The panel was manufactured based on normal practices applied to insulation construction. The composite insulation panel assembly consisted of a warm side layer of polyurethane foam (PUF, ~0.1 m thick) and a cold side layer of phenolic resin foam (PRF, ~0.2 m thick). The assembly size was 1m x 1m. There was a steel wire net (mesh) between the PUF and PRF. A thin layer of aluminum sheet was attached to the exterior side (warm side). All materials were formed into a complete assembly (a total thickness of ~0.3 m) with the panel bolted to a 22 mm thick aluminum plate (representing the cargo tank).

The Moss composite panel configuration included a heated area of 1000 mm x 1000 mm (the steel weather cover, ~16 mm), a gap between the weather cover and the insulation system (~1280 mm), the composite panel insulation system (~300 mm thick), the aluminum cryogenic tank (38 mm wall thickness), and the polystyrene insulation on aluminum tank back side (300 mm).

Small diameter holes (~3 mm) were drilled into the foam to depths appropriate for the location of thermocouples. Depending on the location, one or two thermocouples were inserted to the correct depth and glued in place using a bi-component polyurethane-based adhesive. Thermocouples were epoxyed onto the face of the aluminum sheet.

Figure 7 provides photographs of the composite panel assembly. It shows the composite panel as delivered, the guide for drilling TC holes, the TC runs on panel side, and the completed TC installation with the attachment of the panel to the aluminum tank.

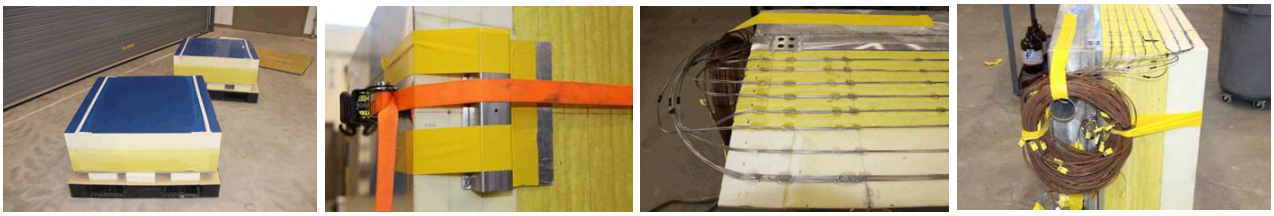

Figure 7. Moss Composite Panel Insulation System Assembly.

Polystyrene Panel Procurement and Instrumentation

Procurement of the extruded polystyrene (EPS) foam panel was facilitated by Moss Maritime AS. The completed panel was shipped directly to Sandia from the manufacturer's facility. The EPS insulation panel assembly consists of 3 layers of polystyrene foam panel, with a total thickness of ~300mm. The assembly size was 1m x 1m. There were 2 intermediate thin layers of glass fiber mesh (crack barrier). And a thin layer of aluminum sheet was glued on the exterior side (warm side) of the insulation. All materials were laminated together to form a complete assembly/composite sandwich using 2-component cryogenic PU adhesive for the lamination.

The polystyrene panel configuration included a heated area of 1000 mm x 1000 mm (the steel weather cover, ~16 mm), a gap between the weather cover and the insulation system (~1382 mm), the polystyrene panel insulation system (~300 mm thick), the aluminum cryogenic tank (38 mm wall thickness), and the polystyrene insulation on aluminum tank back side (300 mm).

Four pre-drilled holes were used to bolt the panel assembly to an aluminum plate (bolts/nuts/washers and aluminum plate were supplied by Sandia). Polystyrene plugs with preattached aluminum sheet were also provided for insertion of the plugs inside the pre-drilled holes after the panel assembly was bolted to the aluminum plate. The aluminum plate (~19 mm thick, (0.75 inch)) had threaded rods for attachment to the polystyrene panel. After the panel was bolted to the plate, the four EPS plugs were glued in place using the bi-component polyurethane-based adhesive. As before, small diameter holes (~3 mm) were drilled into the foam to depths appropriate for the location of thermocouples. Depending on the location, one or two thermocouples were inserted to the correct depth and glued in place. The thermocouples were epoxyed on the face aluminum sheet. As before, many thermocouples were installed on multiple planes within the insulation.

Figure 8 shows the polystyrene insulation panel as delivered, a close-up of the TC installation, the insulation divided into nine thermocouple measurement planes, and the final assembly.

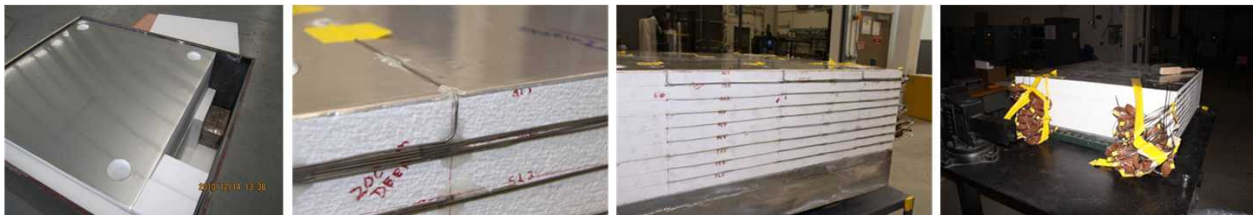

Figure 8. Moss Polystyrene Panel Insulation System Assembly.

Insulation System Test Results

To conduct an insulation thermal damage test, an instrumented insulation system was placed in the test enclosure. Figure 9 shows the instrumented outer hull (or weather cover) installed at the front (heated side) of the test enclosure, an insulation system ready for installation at the rear of the test enclosure, and the front of the test enclosure with the radiometer set to measure the heat flux from the radiant lamp assembly.

Figure 9. Placing an Insulation System Into the Test Enclosure.

Prior to testing, to approximate initial and boundary conditions, a nitrogen gas purge was started and cryogenic nitrogen (liquid and/or gas) was added to the aluminum tank to cool down the insulation panel to near steady-state operational conditions.

At the start of the test, the power to the lamps was rapidly increased until the incident heat flux to the steel plate (as measured by the radiometer) approached 270 kW/m^2. This value was based on the preliminary analysis of the average steady-state surface emissive power measured in the large-scale LNG pool fire test (83 m diameter spreading pool) conducted at Sandia in December 2009 [Blanchat et al. 2011]. The power was adjusted throughout the test as necessary to maintain the desired flux condition. All tests were conducted for a minimum 40 minute duration, based on the latest information on the maximum duration of a large scale LNG spills (accidents or intentional events) and fires [Luketa et al., 2008].

While individual test results are proprietary, based on agreements with the manufacturers to provide proprietary test materials and specifications to Sandia, the following figures can be used to provide examples of the types of results that were obtained from the insulation testing program.

Figure 10 shows the ~40 hour cool down of a typical insulation panel (the averages of the six thermocouples located at eleven planes). The cool down was limited to <20°C/hour through a combination of gas service for the 1st 7 hours and then by small additions (and subsequent boil off) of LN_2 into the tank until the tank approached -196°C after which it was filled and maintained full.

Two nitrogen gas purge lines entered the enclosure, one about mid-depth of the insulation system and one between the weather cover and the insulation system. At the start of the cool down, a small flow (5 LPM) was set at the insulation system inlet. The morning of the test, a larger flow (~2 CFM) was set at the enclosure inlet. These flow rates were designed to reduce the oxygen content inside the insulation system and enclosure to less than 6%.

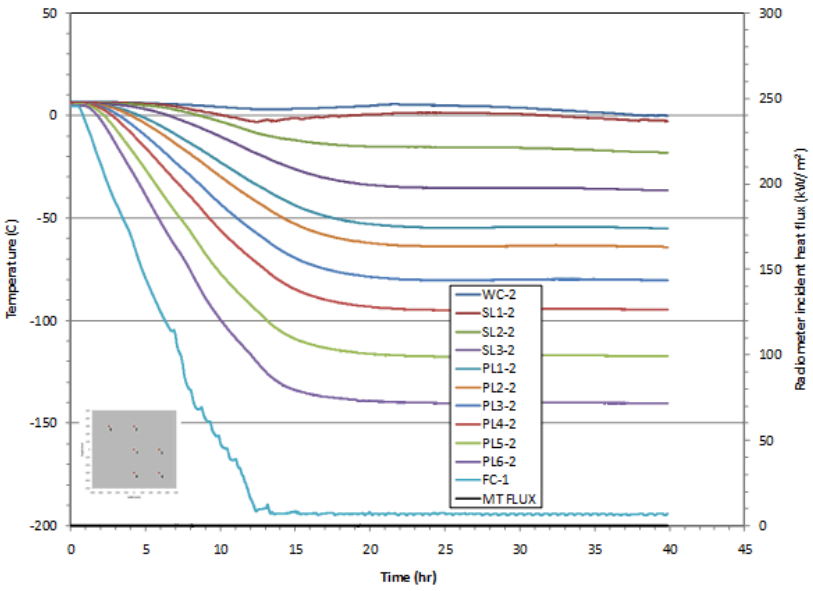

Figure 10. Cool Down of an Insulation System Inside the Test Enclosure.

To start the thermal heating of the insulation system, the four lamp assemblies were then energized in a manually-operated power mode. Figure 11 shows the temperature response (average of the six thermocouples) on each of the eleven planes for a typical test. In addition, the figures plot the heat flux (~270 kW/m^2) that was applied for ~40 minutes to the weather cover/outer hull.

Smoke (from pyrolysis of the insulation materials) and flames were often seen ~5-10 minutes into the test at the exhaust stack (the ignition source was a glow plug igniter attached to the stack exhaust). No flames were seen at the perimeter of the test enclosure due to the relatively tight attachment of the weather cover/outer hull to the enclosure frame and the N_2 purge gas (~2 cubic feet per minute). Figure 11 shows the thermal wave moving through the insulation materials, and in this example, this thermal front arrived at the last thermal couple location, layer (PL6), when the lamps were deenergized at 40 minutes. After the lamps were turned off, the insulation temperatures start to drop off as shown in Figure 11, but the system can take several hours to reduce to ambient conditions. LN_2 was allowed to boil off; the level reached thermocouple FC-1 attached to the aluminum tank at about 2 hours resulting in a small temperature increase.

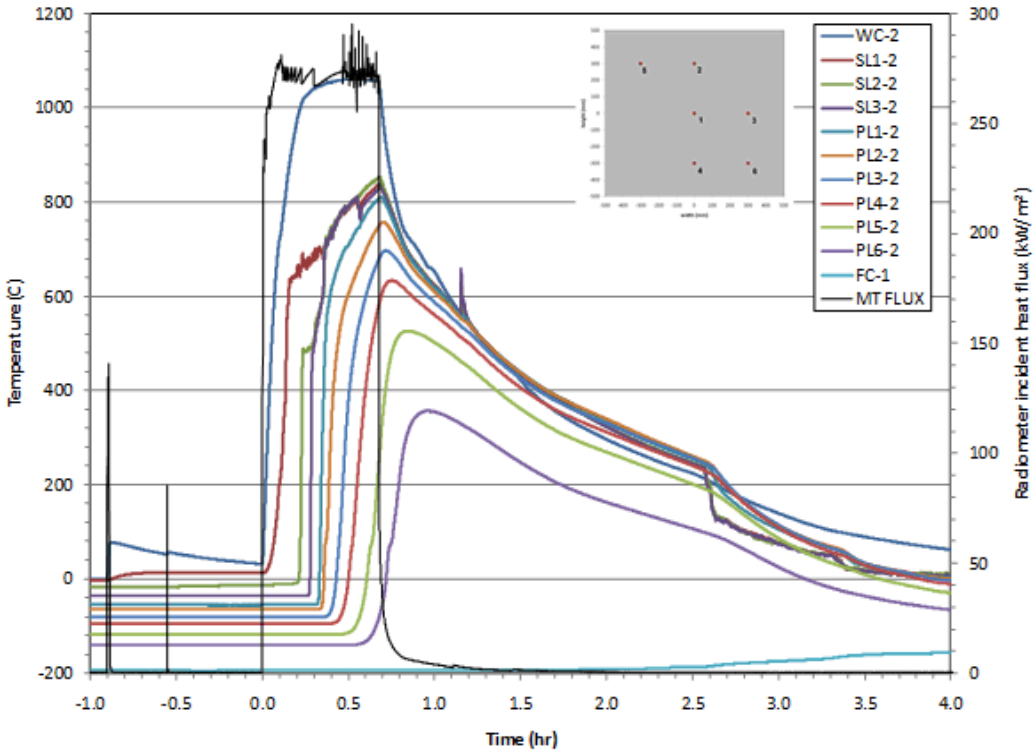

Figure 11. The Thermal Response of an Insulation System.

Note that the steel plate acting as a weather cover/outer hull (WC-2) temperature approached 1100°C and the insulation layers closest to the weather cover/outer hull have reached 800°C near the end of the test.

In general, there was negligible heat flux into the aluminum tank that represents the cargo tank during any of the tests. Only after the thermal front passed through the layer closest to the aluminum tank (PL6) was there an increase in flux. The RdF gauge showed a peak flux of about ~0.5 kW/m^2 about one hour after the lamps were turned off for this test. The LN_2 boil off was also used in all tests to determine a heat flux into the cargo tank. This is done by subtracting the steady-state mass loss rate measured before the test, and multiplying the result by the latent heat of LN_2 (200 kJ/kg) and dividing by the tank front surface area (1 m^2). This method also resulted in a peak flux of ~0.5 kW/m^2. In all tests, the RdF gauge and the LN_2 loss rate measurements provided similar results for maximum heat flux into the cargo tanks.

A summary of all the insulation test results are shown in Table 2. As discussed, the heat flux value shown into the LN_2 tank is an average of values measured by heat flux gauges attached to the tank and by evaluating the change in the liquid nitrogen boil-off rate in the LN_2 tank. While actual heat flux values are available for each insulation material tested, that data is proprietary. The data in Table 2 provides general engineering data on expected heat flux into the different cargo tanks that can be used to assess the potential for cargo tank pressurization and relief valve operational needs in the case of a large LNG spill and fire.

Table 2. LNG Cargo Tank Insulation System Fire Damage Test Results

LNG Vessel	**Insulation Type**	**Thickness**	**Time for Thermal Front to Reach LN_2 Tank**	**LN_2 Tank Heat Flux**
Moss	Extruded polystyrene panel	~300 mm	< 40 min	< 7 kW/m^2
Moss	Polyurethane foam/ phenolic resin foam composite panel	~300 mm	> 40 min	< 5 kW/m^2
Membrane	Polyurethane foam and plywood panel	~300 mm	> 40 min	< 5 kW/m^2
Membrane	Perlite-filled plywood boxes	~500 mm	> 40 min	< 5 kW/m^2

Cascading Damage from LNG Pool Fire – Potential for Overpressure or Thermal Damage to Adjacent Cargo Tanks

Moss

The polystyrene insulation system provides the bounding case for Moss tanks for damage from an LNG spill and pool fire. Styrene has a relatively low ablation temperature, causing it to vaporize more quickly than most other systems. As a consequence, damage to that insulation system was more extensive than other systems, as shown in Table 2.

The thermal wave progression through the polystyrene insulation system was clearly observed. For each location in the system, the temperature remained flat and then suddenly rose as the material vaporizes. This behavior is typical of ablating (or decomposing) insulation. The phase change of the insulation material as it melts, vaporizes, or decomposes consumes effectively all of the energy transferred onto the surface of the insulation from the hot weather cover. Heat transfer into the insulation occurs slowly enough that it arrives at a location with the ablation front. This behavior, an abrupt change in the slope of the temperature response from horizontal to effectively vertical, explains why the measured heat flux into the LN_2 tank is essentially zero until the insulation is gone.

Prior to the conclusion of the polystyrene test, the last layer of insulation vaporized and the thermal wave reached the tank. The heat flux into the LN_2 tank was expected to increase dramatically (at that time the hot weather cover was ~1100°C, and assuming an emissivity of 0.85-0.9 (reasonable for a sooted surface) a heat flux of ~170-190 kW/m^2 was anticipated; however, the measured heat flux into the tank was <7 kW/m^2.

On ablation, the styrene either vaporizes or forms soot. Video of the exhaust from the fixture during the test showed that the amount of soot formed was significant. Unfortunately, the experiment design did not allow for quantification of the fraction of styrene that forms soot.

It was postulated that this result was due primarily to the presence of smoke within the inerted space, which reduces the radiative heat transfer from the weather cover to the tank wall. This hypothesis was explored using approximate solutions to the radiative transfer equation for participating media between isothermal infinite parallel planes and confirmed; soot can account for a dramatic reduction in radiant energy transferred between the weather cover and the wall of the tank. At the expected concentrations of ~100 ppm the computed radiative heat flux was lower than the measured heat flux. The measured heat flux could be matched by adjusting the assumed soot volume fraction, but the temperature distribution would not match the experiment. This suggests that convection may play an important role in this scenario, circulating fluid through the box in a convective cell that increases the heat fluxes on the tank wall and changes the temperature distribution in the box.

In considering both a participating media heat transfer analysis and a free convection heat transfer analysis for a Moss LNG cargo tank, those analyses support a likely maximum heat flux estimate of up to 10 kW/m^2 onto the cargo tank (Morrow 2011). Based on the fire modeling information and heat transfer analysis, these heat flux values can be assumed to occur during free convection over the full tank surface area, including the area of the cargo tank below the main deck of the LNG vessel. Therefore, there is a possibility that the entire tank could see a heat flux of up to 10 kW/m^2, not just that portion of the tank above the water line directly exposed to a fire.

There has been much discussion on the impacts of a large LNG pool fire on increasing vaporization of LNG in undamaged tanks and the capacity of the current pressure safety relief valves to handle this increased vaporization. The concern is that if pressure builds up during a fire and cannot be adequately handled by the pressure safety relief valve systems, then a cargo tank could become over-pressurized, fail, lead to additional LNG spills, larger fires, and increase hazards to property and the public.

From our the analyses, a heat flux of about 5 kW/m² will result in an average pressure equivalent to the normal operating pressure of a Moss cargo tank of ~1.3 psig. A heat flux of 10 kW/m^2 will result in an average pressure of ~2.8 psig, and for the free convection case, a pressure of ~14.7 psig. Moss LNG cargo tanks are constructed to a design pressure which significantly exceeds the highest estimated pressure from the above scenarios. While the increased heat flux will cause some vaporization of the LNG in the vessel's cargo tanks, the cargo tank pressure relief valves are adequately sized to handle the resulting vapor production rates. Due to the combination of adequately sized cargo tank pressure relief valves and cargo tank design standards, there is a minimal likelihood of a Moss LNG cargo tank being damaged from a fire due to vapor over pressurization.

Our analysis approach was compared to an analysis performed by the Society of International Gas Tanker and Terminal Operators (SIGTTO) in 2009. This was an industry-wide study conducted to assess LNG cargo tank safety relief valve performance in the face of a large pool fire. The SIGTTO approach used standard handbook sizing algorithms and simplifying assumptions on fire/vessel interactions and cargo tank insulation damage rates, but reached similar conclusions. Overall, the testing and analyses suggest that the Moss LNG cargo tank insulation materials currently used can provide protection of the other cargo tanks in a fire, and LNG vaporization in those tanks would not increase to a level that would exceed the pressure safety relief valve capacity or damage the other cargo tanks.

The tests and subsequent analyses demonstrated that for Moss Maritime type spherical cargo tanks the LNG pool fire heat flux imposes minor additional risks from cascading damage to adjacent tanks. The weather covers over the tanks will experience high temperatures – high enough to cause sagging and the cargo tanks' insulation systems will be damaged. However, the cargo tanks' aluminum walls will not experience excess temperature. The affected tanks' relief valves will lift, releasing methane vapor into the fire. However, the tanks will not overpressure.

Membrane

As with the Moss style systems, the outer steel surfaces will see very high temperatures. In our experiments, the outer hull reached temperatures close to 1100ºC. At these temperatures, the hull steel will lose structural integrity, but as shown in Table 2, the heat flux into the LN_2 tank was very low, and the thermal wave for both membrane insulation systems had not reached the LN_2 tank at the end of the nominal 40 minute thermal tests.

The volume between the outer and inner hulls should contain little material that could vaporize or form soot. However, pressure may increase due to increasing gas temperature in the inter-hull volume. Assuming the average temperature of the vapor in the volume (combined above and below the waterline) increases to 475°C, without venting the pressure would climb to 2.5 atmospheres absolute, or 1.5 atmospheres gauge. The temperature rise takes place over 30 to 40 minutes. This buildup is slow enough that relief valves protecting this area should be capable of venting enough vapors to minimize impact.

Complicating this analysis would be the response of both the outer hull and the inner hull. Both will heat up to the point of losing structural integrity, and will deform in response to increasing pressure. Such deformation could increase the volume between hulls, thereby reducing pressure. But deformation of the inner hull implies a concomitant distortion of the LNG membrane cargo tank support, and therefore the membranes themselves.

The issue of pressure buildup within the membrane system also deserves some attention. The secondary layers of both membrane systems suffered thermal damage. Production and expansion of gases from thermally-decomposing materials will increase pressure internal to the insulation systems; given the relatively small original vapor volume, this pressure increase may exceed the relief and venting capacity of this volume.

Another issue is whether a potential fire would cause an LNG membrane ship's inner and outer hulls or membranes to distort enough to allow wholesale escape of LNG. Inner and outer hull distortion can come from two sources. First, the softening of the outer and inner hulls from a fire, and second, vaporization of the insulation or plywood insulation producing pressure sufficient to deform the membrane. As a consequence, it is likely that some membrane tanks will distort during a large fire.

The membrane itself is built with corrugations designed to allow for thermal expansion. As a consequence the membranes look somewhat like a pleated accordion bellows. Without anchors, this pleating does allow distortion associated with pressure or loss of support to distribute itself across a large area of tank wall. The question is whether the membrane cargo tank will be damaged significantly by a fire before damage to the hulls occur. From our test results and our impact analyses on LNG cargo tank pressurization, our assessment is that distortion of the inner and outer hulls during a large LNG fire will be the larger cascading damage driver for the membrane ships, not the thermal and pressure integrity performance of the membrane LNG cargo tank insulation systems in a large fire scenario.

Conclusions

DOE and the USCG tasked Sandia National Laboratories to perform a set of experiments to address the concern that cryogenic insulation (installed to preserve the cold conditions of LNG cargo) could degrade in the event of a large-scale LNG spill and fire engulfing an LNG carrier. The experiments were aimed at

investigating whether degradation of the insulation systems could cause initially undamaged LNG cargo tanks to become damaged, resulting in additional spills and larger and/or longer fires.

Tests were performed on four large-scale LNG ship cargo tank insulation systems; two representative for membrane-type ships and two representative for Moss-type ships. All tests were performed using Sandia's Thermal Test Complex's large-scale radiant heat capability that allowed identical and reproducible heat flux boundary conditions representative of large LNG fires for each test.

All tests were performed to yield a continuous external heat flux of ~270 kW/m^2 with a minimum duration of 40 minutes. The heat flux magnitude was based on the average steady-state surface emissive power measured in the large-scale LNG pool fire test (83 m diameter spreading pool) conducted at Sandia in December 2009 [Blanchat et al. 2011]. The duration time is the expected credible LNG pool fire duration based on the latest information on large scale LNG spills (accidents or intentional events) and fires as determined by Sandia [Luketa et al. 2008].

All insulation systems showed some thermal degradation, and damage severity varied by insulation type, but overall performed quite well and much better than generally expected in several cases. The maximum heat flux (for all tests) at the surface representing the LNG cargo tank (after passing through the insulation system) was ~5 kW/m^2.

The following key observations were made:

1. Heat flux of ~5 kW/m^2 will not cause high temperature/direct damage of the cargo tank.
2. Simplified and conservative calculations show that the additional boil off due to the largest recorded heat flux of ~5 kW/m^2 does not exceed the venting capacity of the cargo tank relief valves, which means tank pressure will remain below acceptable limits.
3. An external heat flux of 270 kW/m^2 creates high temperatures (~1000-1100°C) on the steel plate representing the external exposed surface (outer hull for the membrane carriers; weather cover for the Moss carriers). The high temperatures measured on the structural steels were sufficient to cause reduction in mechanical strength of the steels that support the membrane cargo tanks or the weather covers for the Moss cargo tanks.
4. The high temperatures experienced by all of the insulation systems were sufficient to cause degradation and reduction in mechanical strength of the insulation systems. The high temperatures seen in the Moss carrier insulation systems do not affect the cargo tank structure integrity, but these temperatures would lead to insulation material pyrolysis, degradation, and flue gas and soot formation in the hold space.

References

American Bureau of Shipping, "Guidance Notes on Surveys during Construction of Membrane Tank LNG Carriers," June 2008.

Blanchat, T., Helmick, P., Jensen, R., Luketa, A., Deola, R., Suo-Anttila, S., Mercier, J., Miller, T., Ricks, A., Simpson, R., Demosthenous, B., Tieszen, S., and Hightower, M., "The Phoenix Series Large Scale LNG Pool Fire Experiments," SAND2010-8676, Sandia National Laboratories, Albuquerque, NM, December 2011.

Hightower, M., Gritzo, L., Luketa-Hanlin, A., Covan, J., et al., "Guidance on Risk Analysis and Safety Implications of a Large Liquefied Natural Gas (LNG) Spill Over Water," SAND2004-6258, Sandia National Laboratories, Albuquerque, NM, December 2004.

Luketa, A., "Recommendations on the prediction of thermal hazard distances from large liquefied natural gas pool fires on water for solid flame models," SAND2011-0495, Sandia National Laboratories, Albuquerque, NM, January 2011.

Luketa, A., Hightower, M., Attaway, S., "Breach and Safety Analysis of Spills Over Water from Large Liquefied Natural Gas Carriers," SAND2008-3153, Albuquerque, NM, May 2008.

Morrow, C., "Cascading Damage from an LNG Pool Fire – Potential for Overpressure or Thermal Damage to Adjacent Cargo Tanks," SAND2012-3000, Albuquerque, NM, April 2012.

Vela, Iris; Chun, Hyunjoo; Wehrstedt, Klaus-Dieter; Schönbucher, Axel, "Thermal radiation of di-tert-butyl peroxide pool fires - Experimental investigation and CFD simulation," Journal of Hazardous Materials, 1, 167, 2009, 105–113.